**This document is downloaded from DR-NTU (https://dr.ntu.edu.sg)**
**Nanyang Technological University, Singapore.**

# Zinc oxide quantum dots embedded films by metal organic chemical vapor deposition

Zhang, X. H.; Chen, B. J.; Chua, S. J.; Dong, Zhili; Hu, Xiao; Tan, Swee Tiam; Sun, Xiaowei; Yong, Anna

2006

Tan, S. T., Sun, X., Zhang, X. H., Chen, B. J., Chua, S. J., Yong, A., et al. (2006). Zinc oxide quantum dots embedded films by metal organic chemical vapor deposition. Journal of Crystal Growth, 290(2), 518-522.

https://hdl.handle.net/10356/95559

https://doi.org/10.1016/j.jcrysgro.2006.02.035

© 2006 Elsevier. This is the author created version of a work that has been peer reviewed and accepted for publication by Journal of Crystal Growth, Elsevier. It incorporates referee’s comments but changes resulting from the publishing process, such as copyediting, structural formatting, may not be reflected in this document. The published version is available at: http://dx.doi.org/10.1016/j.jcrysgro.2006.02.035.

*Downloaded on 20 Mar 2024 17:06:37 SGT*

# Zinc oxide quantum dots embedded films by metal organic chemical vapor deposition

***S.T. Tan[a,b], X.W. Sun[a,*], X.H. Zhang[b], B.J. Chen[a], S.J. Chua[b], Anna Yong[b], Z.L. Dong[c], X. Hu[c]***

[a]*School of Electrical and Electronic Engineering, Nanyang Technological University, Nanyang Avenue, Singapore 639798, Singapore*
[b]*Institute of Materials Research and Engineering, 3 Research Link, Singapore 117602, Singapore*
[c]*School of Materials Engineering, Nanyang Technological University, Nanyang Avenue, Singapore 639798, Singapore*
[*]*Corresponding author.*
*E-mail address: exwsun@ntu.edu.sg (X.W. Sun).*

**Abstract**

Zinc oxide (ZnO) quantum dots (QDs) were fabricated on silicon substrates by metal organic chemical vapor deposition. Formation of QDs is due to the vigorous reaction of the precursors when a large amount of precursors was introduced during the growth. The size of the QDs ranged from 3 to 12 nm, which was estimated by high-resolution transmission electron microscopy. The photoluminescence measured at 80 K showed that the emission of QDs embedded film ranged from 3.0 to 3.6 eV. The broad near-band-edge emission was due to the quantum confinement effect of the QDs.

Keywords: A2. MOCVD; A3. Quantum dots; B1. Nanocrystals; B1. ZnO

## 1. Introduction

Zinc oxide (ZnO) is looked upon as a promising material for the application of short-wavelength opto-electronic devices due to its large direct bandgap of 3.377 eV. Moreover, ZnO has a large exciton binding energy of 60 meV [1], which is much higher than that of GaN (21–25 meV) and ZnSe (22 meV). This makes ZnO much more attractive, as the large exciton binding energy will result in more efficient ultraviolet (UV) emission even at room temperature [2,3]. The nanostructures of the ZnO material have also been investigated intensively recently. In fact, ZnO shows the richest nanostructural morphologies of all materials. Among these ZnO nanostructures, nanowire [4], nanorod [5], nanopin [6], nanoring [7], nanodisk [8], and quantum dots (QDs) [9,10], have been fabricated and investigated.

It is expected that the significance of the exciton effects will become more prominent in nanostructure materials especially in zero-dimensional nanostructures, i.e. QDs. Hence, QDs are expected to have many interesting and useful properties for opto-electronic applications, for example, QDs in semiconductor laser application, which was firstly proposed by Arakawa and Sakaki [11] in 1982. In this paper, we shall report the fabrication of ZnO QDs embedded film and discuss the dependency of QDs bandgap on dot size prepared by metal organic chemical vapor deposition (MOCVD).

## 2. Experimental procedure

The ZnO QDs used in this paper were grown on Si(1 0 0) by MOCVD. The Si wafer was cleaned by sequential ultrasonic baths of acetone, ethanol, and rinsed by de-ionized water. Hence, it is expected that a thin layer of oxide will form on the Si wafer especially the wafer was heated up in the reactor chamber with the presence of $O_2$. The growth temperature was set at 350 ℃. DimethylZinc (DMZn), $N_2$ gas and high-purity $O_2$ were used as the zinc source, carrier gas and oxidizing agent, respectively. The flow rates of the DMZn ($N_2$ carrier gas) and $O_2$ were set at 20 sccm each for the QDs fabrication. The DMZn bubbler was kept at −10 ℃ in a coolant water bath. The chamber pressure was maintained at about 30 mbar and the deposition time was 10 min. The QDs embedded ZnO films grown at 350 ℃ have an average thickness of 290 nm. The sample used in this study has a thickness of 280 nm that confirmed by the surface profile measuring system (TENCOR P-10). For comparison purpose, a highly *c*-axis oriented ZnO thin film was grown at 350 ℃ with the flow rate of DMZn ($N_2$ carrier gas) and $O_2$ maintained at 3 sccm each. Besides the precursors flow rate, the experiment conditions for growing ZnO QDs and highly *c*-axis oriented ZnO thin films were exactly the same. The highly *c*-axis oriented ZnO thin film has a thickness of 260 nm. The growth rate for highly *c*-axis oriented films is comparable to that of QDs embedded films indicates the excess precursors used in the later growth. In fact, after the growth of QDs embedded films, the stainless steel wall of the reactor chamber was covered with a layer of white particles, which was confirmed as ZnO powder. The crystal structure of the obtained films was characterized by X-ray diffraction (XRD) measurement with CuKα radiation (Siemens D5005 X-ray Diffractometer). High-resolution transmission electron microscopy (HRTEM) with accelerating voltage of 300 kV was employed to observe the lattice structure (JEOL 3010). Photoluminescence (PL) of the ZnO films was measured with a micro-PL system excited with a 325 nm line He-Cd laser of 30 mW and detected with a charge-coupled device (CCD) array at a temperature of 80K.

## 3. Results and discussion

Fig. 1(a) and (b) show the XRD profiles of ZnO thin film grown at 3 and 20 sccm of DMZn and $O_2$ each, respectively. From Fig. 1(a), it can be seen that the ZnO film exhibits highly *c*-axis oriented structures, while the crystallinity of the QDs embedded film was poor and exhibits polycrystalline structures with the existence of various crystallographic planes, as shown in Fig. 1(b). By using Scherrer's formula [12], the grain size corresponding to crystallographic plane (1 0 0), (0 0 2), and (1 0 1) was estimated to be 3.45, 9.92, and 4.83 nm, respectively.

Fig. 2(a) shows the HRTEM image for the ZnO film grown with DMZn and $O_2$ at a flow rate of 20 sccm each. As seen from Fig. 2(a), the QDs are found embedded in the ZnO film grown on Si substrates. The size distribution of ZnO QDs embedded film can be observed clearly in the lower magnification of the HRTEM image, as shown in Fig. 2(b). The QDs were uniformly distributed in the film and the size of the QDs measured was in the range of 3–12 nm. The QDs size was estimated from Fig. 2(b) and the distribution was plotted as histogram as shown in Fig. 3. The dotted curve is the Gaussian fitting of the QDs distribution. Most QDs were distributed at around 7 nm in diameter. The measured QDs sizes are in good agreement with the grain size estimated by using the Scherrer's formula from XRD data.

Fig. 4(a) and (b) show, respectively, the PL of the highly *c*-axis oriented ZnO film and QDs embedded film measured at temperature 80 K. The inset of Fig. 4(b) shows the room temperature PL of QDs embedded film. The PL spectrum of the highly *c*-axis oriented ZnO film shown in Fig. 4(a) is dominated by the near-band-edge emission (NBE) at 3.356 eV, which is attributed to the neutral donor-bound exciton ($D^0X$). The shoulder peaks at 3.326 and 3.249 eV are attributed to the deep bound

exciton and donor-acceptor pair (DAP) emissions [13,14]. The spectrum, however, shows drastic difference for QDs embedded film, as shown in Fig. 4(b). The emission spectrum of the QDs embedded film measured at 80K shows a broad NBE with a tail up to 3.6 eV and peaking at around 3.358 eV, which is attributed to $D^0X$. As the transverse optical (TO) and longitudinal optical (LO) phonon energy is 51.3 and 71.9 meV [15], respectively, the shoulder peaks observed on the spectrum (Fig. 4(b)) are clearly not the phonon-assisted emission. Since the room temperature PL of the QDs embedded film also exhibits several peaks [Fig. 4(b) inset], we believed that these shoulder peaks are due to the interference effect from the coating of CCD detector. However, comparing the PL of QDs embedded film measured at 80 K and room temperature [Fig. 4(b)], there is an obvious change in the NBE shape. At temperature of 80K, the emission peaks at 3.358 eV ($D^0X$) and 3.509 eV can be identified even with the presence of the interference noise.

The quantum confinement effect of the band tail emission could be observed from PL measurement and the size-dependence of the QDs bandgap ($E_{(gap,QDs)}$) can be described by the following equation [10,16]:

$$E_{(gap,QDs)} = E_{(gap,bulk)} + \frac{\pi^2\hbar^2}{2R^2}\left(\frac{1}{m_e^*} + \frac{1}{m_h^*}\right) - 0.248E_{Ryd}^*. \quad (1)$$

The bulk bandgap, $E_{(gap,bulk)}$ is taken as 3.377 eV and the bulk exciton binding energy, $E_{Ryd}^*$ is taken as 60 meV. According to Beni and Rice [17] and Fan et al. [18], the electron and hole effective masses are taken as $m_e^* = 0.24m_0$ and $m_h^* = 2.31m_0$, respectively. Additionally, $\hbar$ is the Planck's constant and R is the radius of ZnO QDs. Using Eq. (1), the QDs bandgap ($E_{(gap,QDs)}$) of the dot size of 3–12 nm was calculated to be 4.130–3.425 eV, respectively. Owing to the fact that Eq. (1) was derived with the assumption that the electrons and holes are completely confined in the well by the infinite potential barrier, the actual quantum confinement effect should be less significant, as is seen in Fig. 4(b). Besides, due to the presence of smaller percentage of 3 nm QDs, as shown in Fig. 3, their contribution to the emission is weak. Hence, its corresponding emission could not be observed in the PL measurement. Meanwhile, for the most distributed QDs with diameter of 7nm shown in Fig. 3, the corresponding emission calculated was 3.503 eV. It can be seen from Fig. 4(b) that the emission peak at 3.509 eV, due to 7 nm QDs, can be clearly identified even with the presence of interference.

Other than the NBE, the deep-level emission (DLE) was observed for both the highly *c*-axis oriented and QDs embedded ZnO films as shown in Fig. 4. The DLE for highly *c*-axis oriented ZnO film peaking at 2.5 eV while the QDs embedded film has a DLE centered at 2.26 eV. It is generally well accepted that the DLE at around visible spectrum is attributed to the recombination of a photo-generated hole with an electron in singly ionized oxygen vacancy in ZnO films [10,19,20]. The ratio of NBE to DLE is generally used to evaluate the concentration of structural defects in ZnO films. The NBE to DLE ratio of the highly *c*-axis oriented film is 17 while for the QDs embedded film is only about 2. The PL efficiency of the QDs embedded films is inferior, which is expected. The incorporation of the nanocrystals deteriorates the crystallinity of the films, which in turn degrades the luminescence efficiency. The defects concentration is expected to be higher in the QDs embedded films compared to highly *c*-axis oriented film. Moreover, with a comparable thickness of both samples, the PL of the QDs embedded film is much inferior due to the fact that the amorphous ZnO (matrix) should not emit well [12].

The relative quantum yield of the highly *c*-axis oriented and QDs embedded ZnO films was estimated by integrating the area under the PL spectra. The quantum yield of the QDs embedded film

is around 5% of that of the highly *c*-axis oriented ZnO films. The quantum yield is low due to the fact that the QDs embedded films are poor in crystallinity. Also, it is worth mentioning that, the QDs embedded film is in the form of ZnO nanocrystals embedded in the ZnO amorphous matrix, i.e. ZnO amorphous phase is dominant compared to the QDs. As a result, the PL quantum yield of the QDs embedded film is definitely lower than that of the highly *c*-axis oriented one, as the amorphous phase does not emit well [12].

From the XRD measurement, it can be seen that, as the precursors flow rate increased from 3 to 20 sccm each, the film crystallinity impaired significantly. We believe that the QDs are formed in gaseous phase and then incorporated into the ZnO film during the growth. The growth mechanism is illustrated in Fig. 5. It is well known that the DMZn will react vigorously with oxygen even at room temperature [21]. Hence, the pre-reaction of the precursors can easily happen during the growth, especially when a large amount of precursors is introduced into the chamber, as shown in Fig. 5. The pre-reaction of the precursors in gaseous phase facilitates the formation of nanocrystals, which is then incorporated into the ZnO film (Fig. 5(b)). The QDs formed in gaseous phase and incorporated in the film during the growth, resulting in poor film crystallinity, as shown in Fig. 1(b). Also, as the incorporation of the ZnO QDs takes place randomly, the various crystallographic planes were formed and detected, which are similar to ZnO powders detection [22]. In fact, the white ZnO nanocrystals were deposited on the stainless steel wall of the reactor chamber after the experiment. The formation of QDs embedded in film grown on quartz and sapphire substrates was also observed in our previous work [12,23]. Hence, it is very clear that the formation of QDs is independent of the substrates. This acts as a strong evidence that the QDs are formed in gaseous phase, which is due to the pre-reaction of the precursors.

## 4. Conclusions

In summary, the ZnO QDs embedded film was fabricated by MOCVD. The QDs formation is due to the vigorous reaction of the precursors. The QDs size ranged from 3 to 12 nm was found embedded in film from the HRTEM characterization. The PL spectrum measured at 80K shows that the broadening of NBE with a tail up to 3.6 eV is due to the quantum confinement effect of the QDs.

## Acknowledgements

The authors gratefully acknowledge the sponsorship from Agency for Science, Technology and Research (#0421010010), Singapore. S.T. Tan would like to thank the Institute of Materials Research and Engineering, Singapore for the Postgraduate Scholarship award.

## References


[1] X.W. Sun, H.S. Kwok, J. Appl. Phys. 86 (1999) 408.

[2] R.F. Service, Science 276 (1997) 895.

[3] X.W. Sun, S.F. Yu, C.X. Xu, C. Yuen, B.J. Chen, S. Li, Jpn. J. Appl. Phys. Part II 42 (2003) L1229.

[4] M.H. Huang, S. Mao, H. Feick, H. Yan, Y. Wu, H. Kind, E. Weber, R. Russo, P. Yang, Science 292 (2001) 1897.

[5] B.P. Zhang, N.T. Binh, Y. Segawa, Y. Kashiwaba, K. Haga, Appl. Phys. Lett. 84 (2004) 586.

[6] C.X. Xu, X.W. Sun, Appl. Phys. Lett. 83 (2003) 3806.

[7] Z.L. Wang, Mater. Today 7 (2004) 26.

[8] C.X. Xu, X.W. Sun, Z.L. Dong, M.B. Yu, Appl. Phys. Lett. 85 (2004) 3878.

[9] S.W. Kim, S. Fujita, S. Fujita, Appl. Phys. Lett. 81 (2002) 5036.

[10] K.K. Kim, N. Koguchi, Y.W. Ok, T.Y. Seong, S.J. Park, Appl. Phys. Lett. 84 (2004) 3810.

[11] Y. Arakawa, H. Sakaki, Appl. Phys. Lett. 40 (1982) 939.

[12] S.T. Tan, B.J. Chen, X.W. Sun, W.J. Fan, H.S. Kwok, X.H. Zhang, S.J. Chua, J. Appl. Phys. 98 (2005) 013505.

[13] D.C. Look, D.C. Reynolds, C.W. Litton, R.L. Jones, D.B. Eason, G. Cantwell, Appl. Phys. Lett. 81 (2002) 1830.

[14] A.B.M.A. Ashrafi, I. Suemune, H. Kumano, S. Tanaka, Jpn. J. Appl. Phys. 41 (2002) L1281.

[15] Y. Zhang, B. Lin, X. Sun, Z. Fu, Appl. Phys. Lett. 86 (2005) 131910.

[16] Y. Kayanuma, Phys. Rev. B 38 (1988) 9797.

[17] G. Beni, T.M. Rice, Phys. Rev. B 18 (1978) 768.

[18] W.J. Fan, J.B. Xia, P.A. Agus, S.T. Tan, S.F. Yu, X.W. Sun, J. Appl. Phys. 99 (2006) 013702.

[19] K. Vanheusden, C.H. Seagar, W.L. Warren, D.R. Tallant, J.A. Voigt, Appl. Phys. Lett. 68 (1996) 403.

[20] S.T. Tan, B.J. Chen, X.W. Sun, M.B. Yu, X.H. Zhang, S.J. Chua, J. Elec. Mater. 34 (2005) 1172.

[21] X. Wang, S. Yang, X. Yang, D. Liu, Y. Zhang, J. Wang, J. Yin, D. Liu, H.C. Ong, G. Du, J. Crystal Growth 243 (2002) 13.

[22] J.I. Langford, A. Boultif, J.P. Auffredic, D. Louer, J. Appl. Crystal 26 (1993) 22.

[23] S.T. Tan, B.J. Chen, X.W. Sun, X. Hu, X.H. Zhang, S.J. Chua, J. Crystal Growth 281 (2005) 571.

**List of figures**

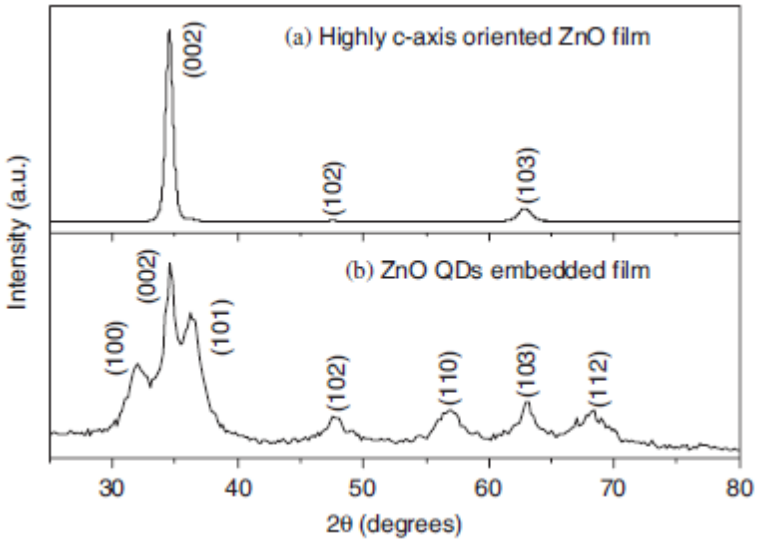
(a) Highly c-axis oriented ZnO film
(002)
(102)
(103)
(b) ZnO QDs embedded film
(100)
(002)
(101)
(102)
(110)
(103)
(112)
Intensity (a.u.)
30
40
50
60
70
80
2θ (degrees)

Figure 1

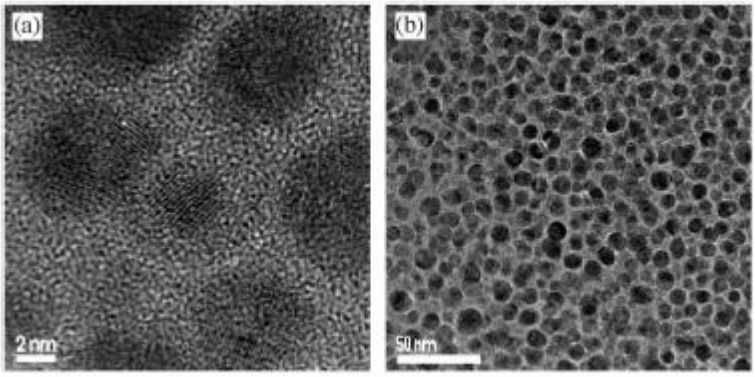


Figure 2

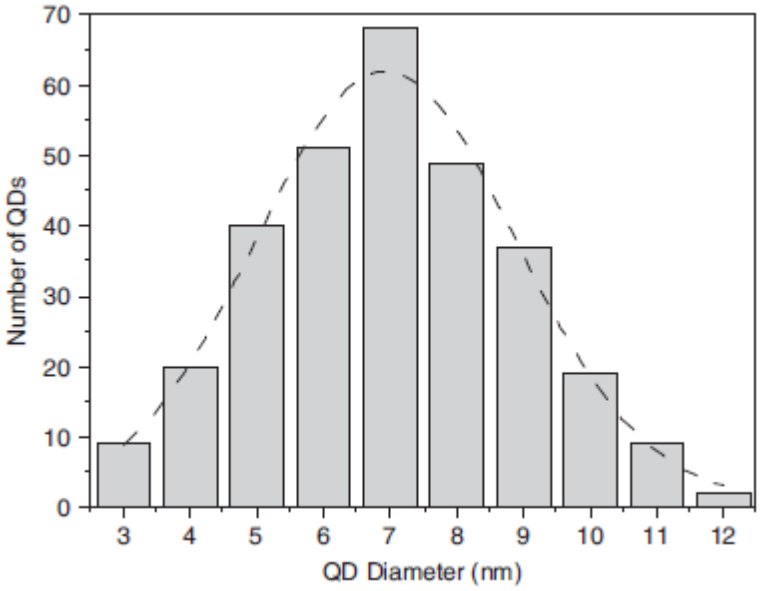
Number of QDs
0
10
20
30
40
50
60
70
3
4
5
6
7
8
9
10
11
12
QD Diameter (nm)

Figure 3

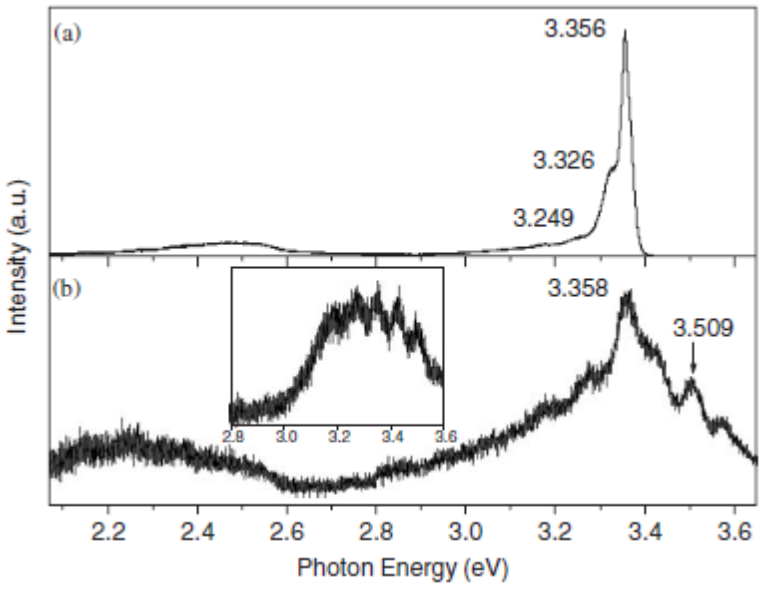
(a)
3.356
3.326
3.249
(b)
3.358
3.509
Intensity (a.u.)
2.2
2.4
2.6
2.8
3.0
3.2
3.4
3.6
Photon Energy (eV)

Figure 4

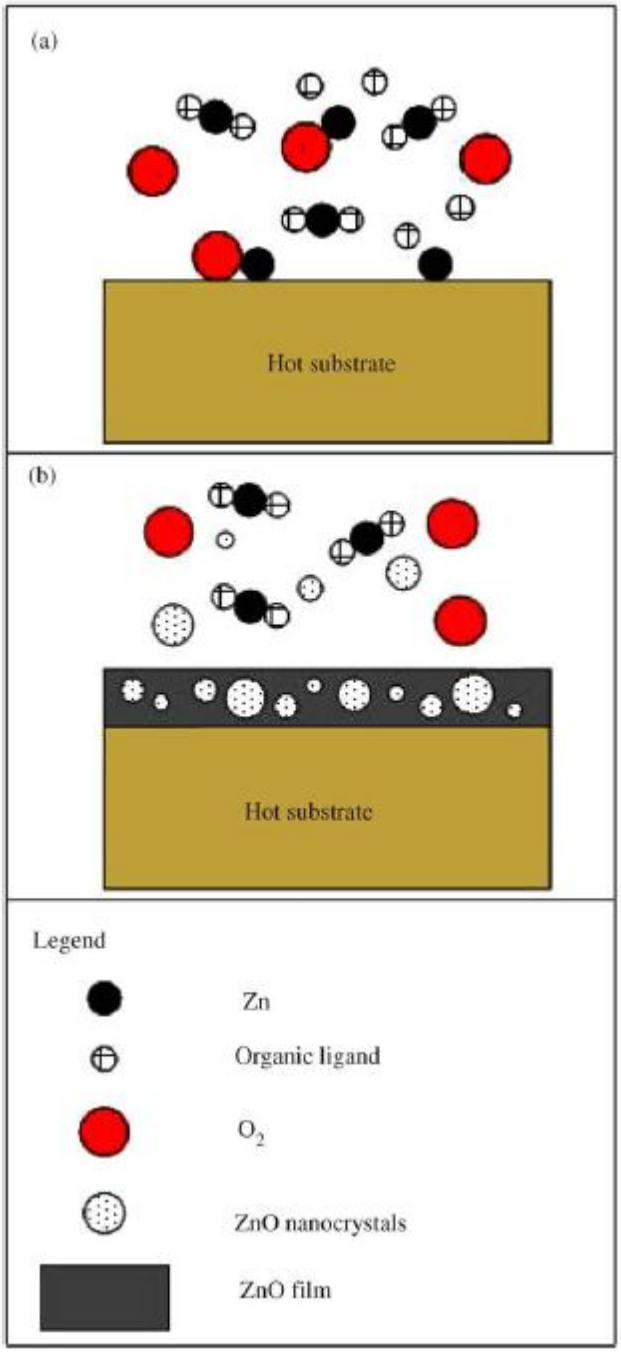
(a)
Hot substrate
(b)
Hot substrate
Legend
Zn
Organic ligand
$O_2$
ZnO nanocrystals
ZnO film

Figure 5